# Heterogeneity in transmissibility and shedding SARS-CoV-2 via droplets and aerosols

Paul Z. Chen[a], Niklas Bobrovitz[b-d], Zahra Premji[e], Marion Koopmans[f], David N. Fisman[g,h], Frank X. Gu[a,i,1]

**Affiliations:**

[a]Department of Chemical Engineering & Applied Chemistry, University of Toronto, Toronto, Canada

[b]Temerty Faculty of Medicine, University of Toronto, Toronto, Canada

[c]Department of Critical Care Medicine, Cumming School of Medicine, University of Calgary, Calgary, Canada

[d]O'Brien Institute of Public Health, University of Calgary, Calgary, Canada

[e]Libraries & Cultural Resources, University of Calgary, Calgary, Canada

[f]Department of Viroscience, Erasmus University Medical Center, Rotterdam, Netherlands

[g]Division of Epidemiology, Dalla Lana School of Public Health, University of Toronto, Toronto, Canada

[h]Division of Infectious Diseases, Temerty Faculty of Medicine, University of Toronto, Toronto, Canada

[i]Institute of Biomedical Engineering, University of Toronto, Toronto, Canada

[1]To whom correspondence may be addressed: Frank X. Gu.

**Email:** f.gu@utoronto.ca

## Abstract

Which virological factors mediate overdispersion in the transmissibility of emerging viruses remains a longstanding question in infectious disease epidemiology. Here, we use systematic review to develop a comprehensive dataset of respiratory viral loads (rVLs) of SARS-CoV-2, SARS-CoV-1 and influenza A(H1N1)pdm09. We then comparatively meta-analyze the data and model individual infectiousness by shedding viable virus via respiratory droplets and aerosols. Our analyses indicate heterogeneity in rVL as an intrinsic virological factor facilitating greater overdispersion for SARS-CoV-2 in the COVID-19 pandemic than A(H1N1)pdm09 in the 2009 influenza pandemic. For COVID-19, case heterogeneity remains broad throughout the infectious period, including for pediatric and asymptomatic infections. Hence, many COVID-19 cases inherently present minimal transmission risk, whereas highly infectious individuals shed tens to thousands of SARS-CoV-2 virions/min via droplets and aerosols while breathing, talking and singing. Coughing increases the contagiousness, especially in close contact, of symptomatic cases relative to asymptomatic ones. Infectiousness tends to be elevated between 1-5 days post-symptom onset. Our findings show how individual case variations influence virus transmissibility and present considerations for disease control in the COVID-19 pandemic.

## Significance Statement

For some emerging infectious diseases, including COVID-19, few cases cause most secondary infections. Others, like influenza A(H1N1)pdm09, spread more homogenously. The virological factors that mediate such distinctions in transmissibility remain unelucidated, prohibiting the development of specific disease control measures. We find that intrinsic case variation in respiratory viral load (rVL) facilitates overdispersion, and superspreading, for COVID-19 but

more homogeneous transmission for A(H1N1)pdm09. We interpret the influence of heterogeneity in rVL on individual infectiousness by modelling likelihoods of shedding viable virus via respiratory droplets and aerosols. We analyze the distribution and kinetics of SARS-CoV-2 rVL, including across age and symptomatology subgroups. Our findings compare individual infectiousness across COVID-19 and A(H1N1)pdm09 cases and present quantitative guidance on triaging COVID-19 contact tracing.

## Main Text

Severe acute respiratory syndrome coronavirus 2 (SARS-CoV-2) has spread globally, causing the coronavirus disease 2019 (COVID-19) pandemic with more than 62.5 million infections and 1.4 million deaths (as of 29 November 2020) (1). For respiratory virus transmission, airway epithelial cells shed virions to the extracellular fluid before atomization (from breathing, talking, singing, coughing and aerosol-generating procedures) partitions them into a polydisperse mixture of particles that are expelled to the ambient environment. Aerosols (≤100 μm) can be inhaled nasally, whereas droplets (>100 μm) tend to be excluded (2, 3). For direct transmission, droplets must be sprayed ballistically onto susceptible tissue (4). Hence, droplets predominantly deposit on nearby surfaces, potentiating indirect transmission. Aerosols can be further categorized based on typical travel characteristics: short-range aerosols (50-100 μm) tend to settle within 2 m; long-range ones (10-50 μm) often travel beyond 2 m based on emission force; and buoyant aerosols (≤10 μm) remain suspended and travel based on airflow profiles for minutes to many hours (4, 5). Although proximity has been associated with infection risk for COVID-19 (6), studies have also suggested that long-range airborne transmission occurs conditionally (7-9).

While the basic reproductive number has been estimated to be 2.0-3.6 (10, 11), transmissibility of SARS-CoV-2 is highly overdispersed (dispersion parameter *k*, 0.10-0.58), with numerous instances of superspreading (7-9) and few cases (10-20%) causing many secondary infections (80%) (12-14). Similarly, few cases drive the transmission of SARS-CoV-1 (*k*, 0.16-0.17) (15), whereas influenza A(H1N1)pdm09 transmits more homogeneously (*k*, 7.4-14.4) (16, 17), despite both viruses spreading by contact, droplets and aerosols (18, 19). Although understanding the determinants of viral overdispersion is crucial towards characterizing transmissibility and developing effective strategies to limit infection (20), mechanistic associations for *k* remain unclear. As an empirical estimate, *k* depends on myriad extrinsic (behavioral, environmental and invention) and host factors. Nonetheless, *k* remains similar across distinct outbreaks (15), suggesting that intrinsic virological factors mediate overdispersion for emerging viruses.

Here, we investigated how intrinsic case variation in rVL facilitates overdispersion in SARS-CoV-2 transmissibility. By systematic review, we developed a comprehensive dataset of rVLs from cases of COVID-19, SARS and A(H1N1)pdm09. Using comparative meta-analyses, we found that heterogeneity in rVL was associated with overdispersion among these emerging infections. To assess potential sources of case heterogeneity, we analyzed SARS-CoV-2 rVLs across age and symptomatology subgroups as well as disease course. To interpret the influence of heterogeneity in rVL on individual infectiousness, we modelled likelihoods of shedding viable virus via respiratory droplets and aerosols.

## Results

### Systematic review

We conducted a systematic review on virus quantitation in respiratory specimens taken during the infectious periods of SARS-CoV-2 (-3 to 10 days from symptom onset [DFSO]) (21-23), SARS-CoV-1 (0-20 DFSO) (24) and A(H1N1)pdm09 (-2 to 9 DFSO) (25) (Methods). The systematic search (*SI Appendix*, Tables S1 to S5) identified 4,274 results. After screening and full-text review, 64 studies met the inclusion criteria and contributed to the systematic dataset (Fig. 1) ($N$ = 9,631 total specimens), which included adult ($N$ = 5,033) and pediatric ($N$ = 1,608) cases from 15 countries and specimen measurements for asymptomatic ($N$ = 2,387), presymptomatic ($N$ = 28) and symptomatic ($N$ = 7,161) infections. According to a hybrid Joanna Briggs Institute critical appraisal checklist, risk of bias was low for most contributing studies (*SI Appendix*, Table S6).

**Association of overdispersion with heterogeneity in rVL**

We hypothesized that individual case variation in rVL facilitates the distinctions in $k$ among COVID-19, SARS and A(H1N1)pdm09. For each study in the systematic dataset, we used specimen measurements (viral RNA concentration in a respiratory specimen) to estimate rVLs (viral RNA concentration in the respiratory tract) (Methods). To investigate the relationship between $k$ and heterogeneity in rVL, we performed a meta-regression using each contributing study (*SI Appendix*, Fig. S1), which showed a weak, negative association between the two variables (meta-regression slope $t$-test: $P$ = 0.038, Pearson's $r$ = -0.26).

Using contributing studies with low risk of bias, meta-regression (Fig. 2) showed a strong, negative association between $k$ and heterogeneity in rVL (meta-regression slope $t$-test: $P < 10^{-9}$, Pearson's $r$ = -0.73). In this case, each unit increase (1 $\log_{10}$ copies/ml) in the standard deviation (SD) of rVL decreased log($k$) by a factor of -1.41 (95% confidence interval [CI]: -1.78 to -1.03),

suggesting that broader heterogeneity in rVL facilitates greater overdispersion in the transmissibility of SARS-CoV-2 than of A(H1N1)pmd09. To investigate mechanistic aspects of this association, we conducted a series of analyses on rVL and then modelled the influence of heterogeneity in rVL on individual infectiousness.

**Meta-analysis and subgroup analyses of rVL**

We first compared rVLs among the emerging infections. We performed a random-effects meta-analysis (*SI Appendix*, Fig. S2), which assessed the expected rVL when encountering a COVID-19, SARS or A(H1N1)pdm09 case during the infectious period. This showed that the expected rVL of SARS-CoV-2 was comparable to that of SARS-CoV-1 (one-sided Welch's *t*-test: $P = 0.111$) but lesser than that of A(H1N1)pdm09 ($P = 0.040$). We also performed random-effects subgroup analyses for COVID-19 (Fig. 3), which showed that expected SARS-CoV-2 rVLs were similar between pediatric and adult cases ($P = 0.476$) and comparable between symptomatic/presymptomatic and asymptomatic infections ($P = 0.090$). Since these meta-analyses had significant between-study heterogeneity among the mean estimates (Cochran's $Q$ test: $P < 0.001$ for each meta-analysis), we conducted risk-of-bias sensitivity analyses; meta-analyses of low-risk-of-bias studies continued to show significant heterogeneity (*SI Appendix*, Figs. S3 to S7).

**Distributions of rVL**

We next analyzed rVL distributions. For all three viruses, rVLs best conformed to Weibull distributions (*SI Appendix*, Fig. S8), and we fitted the entirety of individual sample data for each virus in the systematic dataset (Fig. 4*A* and *SI Appendix*, Fig. S8*N*). While COVID-19 and SARS

cases tended to shed lesser virus than those with A(H1N1)pdm09 (*SI Appendix*, Fig. S2), broad heterogeneity in SARS-CoV-2 and SARS-CoV-1 rVLs inverted this relationship for highly infectious individuals (Fig. 4*A* and *SI Appendix*, Fig. S9 *A* to *C*). At the 90$^{th}$ case percentile (cp) throughout the infectious period, the estimated rVL was 8.91 (95% CI: 8.83-9.00) $\log_{10}$ copies/ml for SARS-CoV-2, whereas it was 8.62 (8.47-8.76) $\log_{10}$ copies/ml for A(H1N1)pdm09 (*SI Appendix*, Table S7). The SD of the overall rVL distribution for SARS-CoV-2 was 2.04 $\log_{10}$ copies/ml, while it was 1.45 $\log_{10}$ copies/ml for A(H1N1)pdm09, showing that heterogeneity in rVL was indeed broader for SARS-CoV-2.

To assess potential sources of heterogeneity in SARS-CoV-2 rVL, we compared rVL distributions among COVID-19 subgroups. In addition to comparable mean estimates (Fig. 3), adult, pediatric, symptomatic/presymptomatic and asymptomatic COVID-19 cases showed similar rVL distributions (Fig. 4 *B* and *C*), with SDs of 2.03, 2.06, 2.00 and 2.01 $\log_{10}$ copies/ml, respectively. Thus, age and symptomatology minimally influenced case variation in SARS-CoV-2 rVL during the infectious period.

**SARS-CoV-2 kinetics during respiratory infection**

To analyze the influences of disease course, we delineated individual SARS-CoV-2 rVLs by DFSO and fitted the mean estimates to a mechanistic model for respiratory virus kinetics (Fig. 4*D* and Methods). The outputs indicated that, on average, each productively infected cell in the airway epithelium shed SARS-CoV-2 at 1.33 (95% CI: 0.74-1.93) copies/ml day$^{-1}$ and infected up to 9.25 susceptible cells (*SI Appendix*, Table S8). The turnover rate for infected epithelial cells was 0.71 (0.26-1.15) days$^{-1}$, while the half-life of SARS-CoV-2 in the respiratory tract was 5.04 (2.62-66.0) hours. By extrapolating the model to an initial rVL of 0 $\log_{10}$ copies/ml, the

estimated incubation period was 5.38 days, which agrees with epidemiological findings (10). Conversely, the expected duration of shedding was 25.1 DFSO. Thus, SARS-CoV-2 rVL increased exponentially after infection, peaked around 1 DFSO along with the proportion of infected epithelial cells (*SI Appendix*, Fig. S10) and then diminished exponentially.

To evaluate case heterogeneity across the infectious period, we fitted distributions for each DFSO (Fig. 4*E*), which showed that high SARS-CoV-2 rVLs also increased from the presymptomatic period, peaked at 1 DFSO and then decreased towards the end of the first week of illness. For the 90$^{th}$ cp at 1 DFSO, the rVL was 9.84 (95% CI: 9.17-10.56) $\log_{10}$ copies/ml, an order of magnitude greater than the overall 90$^{th}$-cp estimate. High rVLs between 1-5 DFSO were elevated above the expected values from the overall rVL distribution (*SI Appendix*, Table S7). At -1 DFSO, the 90$^{th}$-cp rVL was 8.30 (6.88-10.02) $\log_{10}$ copies/ml, while it was 7.93 (7.35-8.56) $\log_{10}$ copies/ml at 10 DFSO. Moreover, heterogeneity in rVL remained broad across the infectious period, with SDs of 1.83-2.44 $\log_{10}$ copies/ml between -1 to 10 DFSO (*SI Appendix*, Fig. S9 *H* to *S*).

**Likelihood that droplets and aerosols contain virions**

Towards analyzing the influence of heterogeneity in rVL on individual infectiousness, we first modelled the likelihood of respiratory particles containing viable SARS-CoV-2. Since rVL is an intensive quantity, the volume fraction of virions is low and viral partitioning coincides with atomization, we used Poisson statistics to model likelihood profiles. To calculate an unbiased estimator of partitioning (the expected number of viable copies per particle), our method multiplied rVL estimates with particle volumes during atomization and an assumed viability proportion of 0.1% in equilibrated particles (Methods).

When expelled by the mean COVID-19 case during the infectious period, respiratory particles showed low likelihoods of carrying viable SARS-CoV-2 (*SI Appendix*, Fig. S11*B*). Aerosols (equilibrium aerodynamic diameter [$d_a$] ≤ 100 μm) were ≤0.69% (95% CI: 0.43-0.95%) likely to contain a virion. Droplets also had low likelihoods: at $d_a$ = 330 μm, they were 19.4% (18.5-20.3%), 2.42% (2.15-2.69%) and 0.20% (0.16-0.24%) likely to contain one, two or three virions, respectively.

COVID-19 cases with high rVLs, however, expelled particles with considerably greater likelihoods of carrying viable copies (Fig. 5 *A* and *B* and *SI Appendix*, Fig. S11 *D* and *E*). For the 80$^{th}$ cp during the infectious period, aerosols ($d_a$ ≤ 100 μm) were ≤36.6% (95% CI: 35.3-38.0%) likely to carry at least one SARS-CoV-2 virion. For the 90$^{th}$ cp, this likelihood was ≤96.7% (96.5-96.9%), with larger aerosols tending to contain multiple virions (*SI Appendix*, Fig. S11*E*). At 1 DFSO, these estimates were greatest, and ≤61.1% (51.8-70.4%) of buoyant aerosols ($d_a$ ≤ 10 μm) contained at least one viable copy of SARS-CoV-2 for the 98$^{th}$ cp. When expelled by high cps, droplets ($d_a$ > 100 μm) tended to contain tens to thousands of SARS-CoV-2 virions (Fig. 5*B* and *SI Appendix*, Fig. S11*E*).

**Shedding SARS-CoV-2 via respiratory droplets and aerosols**

Using the partitioning estimates in conjunction with published profiles of the particles expelled by respiratory activities (*SI Appendix*, Fig. S12), we next modelled the rates at which talking, singing, breathing and coughing shed viable SARS-CoV-2 across $d_a$ (Fig. 5 *C* to *F*). Singing shed virions more rapidly than talking based on the increased emission of aerosols. Voice amplitude, however, had a significant effect on aerosol production, and talking loudly emitted aerosols at similar rates to singing (*SI Appendix*, Fig. S12*E*). Based on the generation of larger

aerosols and droplets, talking and singing shed virions more rapidly than breathing (Fig. 5 *C* to *E*). Each cough shed similar quantities of virions as in a minute of talking (Fig. 5 *C* and *F*).

Each of these respiratory activities expelled aerosols at greater rates than droplets, but particle size correlated with the likelihood of containing virions. Talking, singing and coughing expelled virions at greater proportions via droplets (80.6-86.0%) than aerosols (14.0-19.4%) (Fig. 5*G*). Moreover, short-range aerosols predominantly mediated the virions (90.8-92.6%) shed via aerosols while talking normally and coughing. In comparison, while singing, talking loudly and breathing, buoyant (29.7-68.4%) and long-range (10.3-31.6%) aerosols carried a larger proportion of the virions shed via aerosols (Fig. 5*G*).

**Influence of heterogeneity in rVL on individual infectiousness**

To interpret how heterogeneity in rVL influences individual infectiousness, we modelled total SARS-CoV-2 shedding rates (over all particle sizes) for each respiratory activity (Fig. 5*H* and *SI Appendix*, Fig. S13). Between the 1$^{st}$ and the 99$^{th}$ cps, the estimates for a respiratory activity spanned ≥8.48 orders of magnitude on each DFSO; cumulatively from -1 to 10 DFSO, they spanned 11.0 orders of magnitude. Hence, many COVID-19 cases inherently presented minimal transmission risk, whereas highly infectious individuals shed considerable quantities of SARS-CoV-2. For the 98$^{th}$ cp at 1 DFSO, singing expelled 313 (95% CI: 37.5-3,158) virions/min to the ambient environment, talking emitted 293 (35.1-2,664) virions/min, breathing exhaled 1.54 (0.18-15.5) virions/min and coughing discharged 249 (29.8-2,5111) virions/cough; these estimates were approximately two orders of magnitude greater than those for the 85$^{th}$ cp. For the 98$^{th}$ cp at -1 DFSO, singing shed 14.5 (0.15-4,515) virions/min and breathing exhaled $7.13\times10^{-2}$ ($7.20\times10^{-4}$-22.2) virions/min. The estimates at 9-10 DFSO were similar to these presymptomatic

ones (Fig. 5*H* and *SI Appendix*, Fig. S13*B*). As indicated by comparable mean rVLs (Fig. 3) and heterogeneities in rVL (Fig. 4 *B* and *C*), adult, pediatric, symptomatic/presymptomatic and asymptomatic COVID-19 subgroups presented similar distributions for shedding virions through these activities.

We also compared the influence of case variation on individual infectiousness between A(H1N1)pdm09 and COVID-19. Aerosol spread accounted for approximately half of A(H1N1)pdm09 transmission events (19), and the 50% human infectious dose for aerosolized influenza A virus is approximately 1-3 virions in the absence of neutralizing antibodies (26). Based on the model, 62.9% of A(H1N1)pdm09 cases were infectious (shed ≥1 virion) via aerosols within 24 h of talking loudly or singing (*SI Appendix*, Fig. S14*A*). The estimate was 58.6% within 24 h of talking normally and 22.3% within 24 h of breathing. In comparison, 48.0% of COVID-19 cases shed ≥1 virion via aerosols in 24 h of talking loudly or singing (*SI Appendix*, Fig. S14*C*). Notably, only 61.4% of COVID-19 cases shed ≥1 virion via either droplets or aerosols in 24 h of talking loudly or singing (*SI Appendix*, Fig. S14*D*). While the human infectious dose of SARS-CoV-2 by any exposure route remains unelucidated, it must be at least one viable copy. Thus, at least 38.6% of COVID-19 cases were expected to present negligible risk to spread SARS-CoV-2 through either droplets or aerosols in 24 h. The proportion of inherently infectious cases further decreased as the infectious dose increased: 55.8, 42.5 and 25.0% of COVID-19 cases were expected to shed ≥2, ≥10 and ≥100 virions, respectively, in 24 h of talking loudly or singing during the infectious period.

While these analyses indicated that a greater proportion of A(H1N1)pdm09 cases were inherently infectious, 18.8% of COVID-19 cases shed virions more rapidly than those infected with A(H1N1)pdm09 (Fig. 4*A*). At the 98$^{th}$ cp for A(H1N1)pdm09, singing expelled 4.38 (2.85-

252 6.78) virions/min and breathing exhaled $2.15\times10^{-2}$ ($1.40\times10^{-2}$-$3.34\times10^{-2}$) virions/min. Highly
253 infectious COVID-19 cases expelled virions at rates that were up to 1-2 orders of magnitude
254 greater than their A(H1N1)pdm09 counterparts (Fig. 5*H* and *SI Appendix*, Fig. S15).
255
256 **Discussion**
257 This study provided systematic analyses of several factors characterizing SARS-CoV-2
258 transmissibility. First, we found that broader heterogeneity in rVL facilitates greater
259 overdispersion for SARS-CoV-2 than A(H1N1)pdm09. Our results suggest that many COVID-
260 19 cases infect no one (12-14) because they inherently present minimal transmission risk via
261 droplets or aerosols, although behavioral and environmental factors can further abate risk.
262 Meanwhile, highly infectious cases can shed tens to thousands of SARS-CoV-2 virions/min,
263 especially between 1-5 DFSO. The model estimates, when corrected to copies rather than
264 virions, align with recent clinical findings for exhalation rates of SARS-CoV-2 (27). In
265 comparison, a greater proportion of A(H1N1)pdm09 cases are infectious but shed virions at low
266 rates, which concurs with more uniform transmission and few superspreading events observed
267 during the 2009 H1N1 pandemic (16, 17). Moreover, our analyses suggest that heterogeneity in
268 rVL may be generally associated with overdispersion for viral respiratory infections. In this case,
269 rVL distribution can serve as an early correlate for transmission patterns, including
270 superspreading, during outbreaks of novel respiratory viruses, providing insight for disease
271 control before large-scale epidemiological studies empirically characterize *k*. When transmission
272 is highly overdispersed, targeted interventions may disproportionately mitigate infection (20),
273 with models estimating that focusing half of control efforts on the most infectious 20% of cases
274 outperforms random control policies threefold (15).

Second, we analyzed SARS-CoV-2 kinetics during respiratory infection. While heterogeneity remains broad throughout the infectious period, rVL tends to peak at 1 DFSO and be elevated for 1-5 DFSO, coinciding with the period of highest attack rates observed among close contacts (28). These results indicate that transmission risk tends to be greatest soon after illness rather than in the presymptomatic period, which concurs with large tracing studies (6.4-12.6% of secondary infections from presymptomatic transmission) (29, 30) rather than early temporal models (~44%) (23). Furthermore, our kinetic analysis suggests that, on average, SARS-CoV-2 reaches diagnostic concentrations 1.54-3.17 days after respiratory infection (-3.84 to -2.21 DFSO), assuming assay detection limits of 1-3 $\log_{10}$ copies/ml, respectively, for nasopharyngeal swabs immersed in 1 ml of transport media.

Third, we assessed the relative infectiousness of COVID-19 subgroups. As a common symptom of COVID-19 (31), coughing sheds considerable numbers of virions via droplets and short-range aerosols. Thus, symptomatic infections tend to be more contagious than asymptomatic ones, providing one reason as to why asymptomatic cases transmit SARS-CoV-2 at lower relative rates (32), especially in close contact (33), despite similar rVLs and increased contact patterns. Accordingly, children (48-54% of symptomatic cases present with cough) (34, 35) tend to be less contagious than adults (68-80%) (31, 35) based on tendencies of symptomatology rather than rVL. Conversely, coughing sheds few virions via smaller aerosols. Our analyses suggest that asymptomatic and symptomatic infections present comparable risks for airborne spread, as do adult and pediatric cases. While singing and talking loudly, highly infectious cases shed tens to hundreds of SARS-CoV-2 virions/min via long-range and buoyant aerosols.

297 Our study has limitations. The systematic search found a limited number of studies reporting
298 quantitative specimen measurements from the presymptomatic period, meaning these estimates
299 may be sensitive to sampling bias. Although additional studies have reported semiquantitative
300 metrics (cycle thresholds), these data were excluded because they cannot be compared on an
301 absolute scale due to batch effects (36), limiting use in compound analyses. Furthermore, this
302 study considered population-level estimates of the infectious periods, viability proportions and
303 rate profiles for respiratory particles, which omit individual or environmental variation.
304 Distinctions in phonetic tendencies and, especially for young children, respiratory capacity lead
305 to variation in particle emission rates (37). Some patients shed SARS-CoV-2 with diminishing
306 viability soon after symptom onset (21), whereas others produce replication-competent virus for
307 weeks (38). It remains unclear how case characteristics and environmental factors affect the
308 viability dynamics of SARS-CoV-2.
309 Taken together, our findings provide a potential path forward for disease control. They
310 support aerosol spread as a transmission mode for SARS-CoV-2, including for conditional
311 superspreading by highly infectious cases. However, with short durations of stay in well-
312 ventilated areas, the exposure risk for aerosols, including long-range and buoyant ones, remains
313 correlated with proximity to infectious cases (2, 4). Strategies to abate infection should limit
314 crowd numbers and duration of stay while reinforcing distancing, low voice amplitudes and
315 widespread mask usage; well-ventilated settings can be recognized as lower risk venues.
316 Coughing can shed considerable quantities of virions, while rVL tends to peak at 1 DFSO and
317 can be high throughout the infectious period. Thus, immediate, sustained self-isolation upon
318 illness is crucial to curb transmission from symptomatic cases. Collectively, our analyses
319 highlight the role of cases with high rVLs in propelling the COVID-19 pandemic. While

320 diagnosing COVID-19, qRT-PCR can also triage contact tracing, prioritizing these patients: for
321 nasopharyngeal swabs immersed in 1 ml of transport media, ≥7.14 (95% CI: 7.07-7.22) $\log_{10}$
322 copies/ml corresponds to the top 20% of COVID-19 cases. Doing so may identify asymptomatic
323 and presymptomatic infections more efficiently, a key step towards mitigation as the pandemic
324 continues.

## Materials and Methods

**Systematic review.** We undertook a systematic review and prospectively submitted the protocol for registration on PROSPERO (registration number, CRD42020204637). Other than the title of this study, we have followed PRISMA reporting guidelines (39). The systematic review was conducted according to Cochrane methods guidance (40). In-depth details on the search strategy, selection criteria, data collection and contributing studies are included in the *SI Appendix*, Methods.

**Calculation of rVLs from specimen measurements.** In this study, viral concentrations in respiratory specimens were denoted as specimen measurements, whereas viral concentrations in the respiratory tract were denoted as rVLs. To determine rVLs, each collected quantitative specimen measurement was converted to rVL based on the dilution factor. For example, measurements from swabbed specimens (NPS and OPS) typically report the RNA concentration in viral transport media. Based on the expected uptake volume for swabs (0.128 ± 0.031 ml, mean ± SD) (41) or reported collection volume for expulsed fluid in the study (e.g., 0.5 to 1 ml) along with the reported volume of transport media in the study (e.g., 1 ml), we calculated the dilution factor for each respiratory specimen to estimate the rVL. If the diluent volume was not reported, then the dilution factor was calculated assuming a volume of 1 ml (NPS and OPS), 2 ml (POS and ETA) or 3 ml (NPA) of transport media (42-44). Unless dilution was reported for Spu specimens, we used the specimen measurement as the rVL (21). The non-reporting of diluent volume was noted as an element increasing risk of bias in the hybrid JBI critical appraisal checklist. Specimen measurements (based on instrumentation, calibration, procedures and reagents) are not standardized. While the above procedures (including only quantitative

348 measurements after extraction as an inclusion criterion, considering assay detection limits and
349 correcting for specimen dilution) have considered many of these factors, non-standardization
350 remains an inherent limitation in the variability of specimen measurements.
351
352 **Meta-regression of *k* and heterogeneity in rVL.** To assess the relationship between *k* and
353 heterogeneity in rVL, we performed a univariate meta-regression ($\log k = a(SD) + b$, where $a$
354 is the slope for association and $b$ is the intercept) between pooled estimates of *k* (based on
355 studies describing community transmission) for COVID-19 ($k$ = 0.409) (12-14, 45-48), SARS ($k$
356 = 0.165) (15) and A(H1N1)pdm09 ($k$ = 8.155) (16, 17) and the SD of the rVLs in contributing
357 studies. Since SD was the metric, we used a fixed-effects model. For weighting in the meta-
358 regression, we used the proportion of rVL samples from each study relative to the entire
359 systematic dataset ($W_\mathrm{i} = n_\mathrm{i}/n_\mathrm{total}$). All calculations were performed in units of $\log_{10}$ copies/ml.
360 As the meta-regression used pooled estimates of *k* for each infection, it assumed that there was
361 no correlated bias to *k* across contributing studies. The limit of detection for qRT-PCR
362 instruments used in the included studies did not significantly affect the analysis of heterogeneity
363 in rVL, as these limits tended to be below the values found for specimens with low virus
364 concentrations. The meta-regression was conducted using all contributing studies and showed a
365 weak association. Meta-regression was also conducted using studies that had low risk of bias
366 according to the hybrid JBI critical appraisal checklist and showed a strong association. The *P*-
367 value for association was obtained using the meta-regression slope *t*-test for $a$, the effect
368 estimate.
369

**Meta-analysis of rVLs.** Based on the search design and composition of contributing studies, the meta-analysis overall estimates were the expected SARS-CoV-2, SARS-CoV-1 and A(H1N1)pdm09 rVL when encountering a COVID-19, SARS or A(H1N1)pdm09 case, respectively, during their infectious period. Pooled estimates and 95% CIs for the expected rVL of each virus across their infectious period were calculated using a random-effects meta-analysis (DerSimonian and Laird method). The estimates for rVL assumed that each viral copy was extracted and quantified from the tested specimen aliquot. For studies reporting summary statistics in medians and interquartile or total ranges, we derived estimates of the mean and variance and calculated the 95% CIs (49). All calculations were performed in units of $\log_{10}$ copies/ml. Between-study heterogeneity in meta-analysis was assessed using Cochran's $Q$ test and the $I^2$ and $\tau^2$ statistics. If significant between-study heterogeneity in meta-analyses was encountered, sensitivity analysis based on the risk of bias of contributing studies was performed. The meta-analyses were conducted using STATA 14.2 (StataCorp LLC, College Station, Texas, USA).

**Age and symptomatology subgroup analyses of SARS-CoV-2 rVLs.** The overall estimate for each subgroup was the expected rVL when encountering a case of that subgroup during the infectious period. Studies reporting data exclusively from a subgroup of interest were directly included in the analysis after rVL estimations. For studies in which data for these subgroups constituted only part of its dataset, rVLs from the subgroup were extracted to calculate the mean, variance and 95% CIs. Random-effects meta-analysis was performed as described above. For meta-analyses of pediatric and asymptomatic COVID-19 cases, contributing studies had low risk of bias, and no risk-of-bias sensitivity analyses were performed for these subgroups.

**Distributions of rVL.** We pooled the entirety of individual sample data in the systematic dataset by disease, COVID-19 subgroups and DFSO. For analyses of SARS-CoV-2 dynamics across disease course, we included estimated rVLs from negative qRT-PCR measurements of respiratory specimens for cases that had previously been quantitatively confirmed to have COVID-19. These rVLs were estimated based on the reported assay detection limit in the respective study. Probability plots and modified Kolmogorov–Smirnov tests used the Blom scoring method and were used to determine the suitability of normal, lognormal, gamma and Weibull distributions to describe the distribution of rVLs for SARS-CoV-2, SARS-CoV-1 and A(H1N1)pdm09. For each virus, the data best conformed to Weibull distributions, which is described by the probability density function

$$f(\upsilon) = \frac{\alpha}{\beta}\left(\frac{\upsilon}{\beta}\right)^{\alpha-1} e^{-(\upsilon/\beta)^{\alpha}}, \quad (1)$$

where $\alpha$ is the shape factor, $\beta$ is the scale factor and $\upsilon$ is rVL ($\upsilon \geq 0$ $\log_{10}$ copies/ml). Weibull distributions were fitted on the entirety of collected individual sample data for the respective category. Since individual specimen measurements could not be collected from all studies, there was a small bias on the mean estimate for each fitted distribution. Thus, for the curves shown in Fig. 4, *B* and *C*, the mean of the Weibull distributions summarized in *SI Appendix*, Table S7 was adjusted to be the subgroup meta-analysis estimate for correction; the SD and distribution around that mean remained consistent.

For each Weibull distribution, the value of the rVL at the $x^{\text{th}}$ percentile was determined using the quantile function,

$$\upsilon_x = \beta[-\ln(1-x)]^{1/\alpha}. \quad (2)$$

For cp curves, we used eq. (2) to determine rVLs from the 1st cp to the 99th cp (step size, 1%). Curve fitting to eq. (1) and calculation of eq. (2) and its 95% CI was performed using the Distribution Fitter application in Matlab R2019b (MathWorks, Inc., Natick, Massachusetts, USA).

**Viral kinetics.** To model SARS-CoV-2 kinetics during respiratory infection, we used a mechanistic epithelial cell-limited model for the respiratory tract (50), based on the system of differential equations:

$$\frac{dT}{dt} = -\beta TV \tag{3}$$

$$\frac{dI}{dt} = \beta TV - \delta I \tag{4}$$

$$\frac{dV}{dt} = pI - cV, \tag{5}$$

where $T$ is the number of uninfected target cells, $I$ is the number of productively infected cells, $V$ is the rVL, $\beta$ is the infection rate constant, $p$ is the rate at which airway epithelial cells shed virus to the extracellular fluid, $c$ is the clearance rate of virus and $\delta$ is the clearance rate of productively infected cells. Parameter units are summarized in *SI Appendix*, Table S8. Using these parameters, the viral half-life in the respiratory tract ($t_{1/2} = \ln 2/c$) and the half-life of productively infected cells ($t_{1/2} = \ln 2/\delta$) could be estimated. Moreover, the cellular basic reproductive number (the expected number of secondary infected cells from a single productively infected cell placed in a population of susceptible cells) was calculated by

$$R_{0,c} = \frac{p\beta T_0}{c\delta}, \tag{6}$$

where $T_0$ is the initial number of susceptible cells (50). Further details on fitting procedure and analyses of viral kinetics are included in the *SI Appendix*, Methods.

**Likelihood of respiratory particles containing virions.** To calculate an unbiased estimator for viral partitioning (the expected number of viable copies in an expelled particle at a given size), we multiplied rVLs with the volume equation for spherical particles during atomization and the estimated viability proportion, according to the following equation:

$$\lambda = \frac{\pi \rho v_p \gamma \upsilon}{6} d^3, \quad (7)$$

where $\lambda$ is the expectation value, $\rho$ is the material density of the respiratory particle (997 g/m$^3$), $v_p$ is the volumetric conversion factor (1 ml/g), $\gamma$ is the viability proportion, $\upsilon$ is the rVL and $d$ is the hydrated diameter of the particle during atomization.

The model assumed $\gamma$ was 0.1% as a population-level estimate. For influenza, approximately 0.1% of copies in particles expelled from the respiratory tract represent viable virus (51), which is equivalent to one in 3 $\log_{10}$ copies/ml for rVL or, after dilution in transport media, roughly one in 4 $\log_{10}$ copies/ml for specimen concentration. Respiratory specimens taken from influenza cases show positive cultures for specimen concentrations down to 4 $\log_{10}$ copies/ml (52). Likewise, for COVID-19 cases, recent reports also show culture-positive respiratory specimens with SARS-CoV-2 concentrations down to 4 $\log_{10}$ copies/ml (21), including from pediatric (53) and asymptomatic (22) cases. Our analyses indicated that SARS-CoV-2 rVLs were not different at different sites in the respiratory tract. Moreover, replication-competent SARS-CoV-2 has been found in respiratory specimens taken throughout the respiratory tract (mouth, nasopharynx, oropharynx and lower respiratory tract) (21, 54). Taken together, these considerations suggested that the assumption for viability proportion (0.1%) was

458 suitable to model the likelihood of respiratory particles containing viable SARS-CoV-2. In
459 accordance with the discussion above, the model did not differentiate this population-level
460 viability estimate based on age, symptomatology or sites of atomization. Based on the relative
461 relationship between the residence time of expelled particles before assessment (~5 s) (51), we
462 took the viability proportion (0.1%) to be for equilibrated particles.

463 Likelihood profiles were determined using Poisson statistics, as described by the probability
464 mass function

465 $$\mathrm{P}(X = k) = \frac{\lambda^k e^{-\lambda}}{k!}, \tag{8}$$

466 where $k$ is the number of virions partitioned within the particle. For $\lambda$, 95% CIs were determined
467 using the variance of its rVL estimate. To determine 95% CIs for likelihood profiles from the
468 probability mass function, we used the delta method, which specifies

469 $$\mathrm{Var}\big(g(\boldsymbol{\theta})\big) \approx \sigma^2 \dot{g}(\boldsymbol{\theta})' \mathbf{D} \dot{g}(\boldsymbol{\theta}), \tag{9}$$

470 where $\sigma^2\mathbf{D}$ is the covariance matrix of $\boldsymbol{\theta}$ and $\dot{g}(\boldsymbol{\theta})$ is the gradient of $g(\boldsymbol{\theta})$. For the univariate
471 Poisson distribution, $\sigma^2\mathbf{D} = \lambda$ and

472 $$\dot{g}(\theta) = \frac{\lambda^{k-1} e^{-\lambda}}{k!}(k - \lambda). \tag{10}$$

473

474 **Rate profiles of particles expelled by respiratory activities.** Distributions from the literature
475 were used to determine the rate profiles of particles expelled during respiratory activities. For
476 breathing, talking and coughing, we used data from Johnson et al (55). For singing, we used data
477 from Morawaska et al (56) for smaller aerosols ($d_a$ < 20 μm) and used the profiles from talking
478 for larger aerosols and droplets based on the oral cavity mechanism from Johnson et al (55).
479 Further details on the calculation of rate profiles are included in the *SI Appendix*, Methods. We

480 compared these rate profiles with those collected from talking loudly and talking quietly from
481 Asadi et al (57). After dehydration, the particle diameter becomes approximately 0.5 times the
482 initial size from when atomized in the respiratory tract (55), which was used as the factor
483 between the diameter of hydrated particles during atomization and dehydrated particles.
484 Equilibrium aerodynamic diameter was calculated by $d_a = d_p(\rho/\rho_0)^{1/2}$, where $d_p$ is the
485 dehydrated diameter, $\rho$ is the material density of the respiratory particle (taken to be 1 g/cm$^3$
486 based on the composition of dehydrated respiratory particles) and $\rho_0$ is the reference material
487 density (1 g/cm$^3$). Curves based on discrete particle measurements were connected using the
488 nonparametric Akima spline function.
489
490 **Shedding virions via respiratory droplets and aerosols.** To model the respiratory shedding
491 rate across particle size, rVL estimates and the hydrated diameters of particles expelled by a
492 respiratory activity were input into eq. (7), and the output was then multiplied by the rate profile
493 of the activity (talking, singing, breathing or coughing). To assess the relative contribution of
494 aerosols and droplets to mediating respiratory viral shedding for a given respiratory activity, we
495 calculated the proportion of the cumulative hydrated volumetric rate contributed by buoyant
496 aerosols ($d_a \leq 10$ μm), long-range aerosols (10 μm $< d_a \leq 50$ μm), short-range aerosols (50 μm $<$
497 $d_a \leq 100$ μm) and droplets ($d_a > 10$ μm) for that respiratory activity. Since the Poisson mean was
498 proportional to cumulative volumetric rate, this estimate of the relative contribution of aerosols
499 and droplets to respiratory viral shedding was consistent among viruses and cps in the model.
500 To determine the total respiratory shedding rate for a given respiratory activity across cp, we
501 determined the cumulative hydrated volumetric rate (by summing the hydrated volumetric rates
502 across particle sizes for that respiratory activity) of particle atomization and input it into eq. (7).

Using rVLs and their variances as determined by the Weibull quantile functions, we then calculated the Poisson means and their 95% CIs at the different cps.

To assess the influence of heterogeneity in rVL on individual infectiousness, we first considered transmission of A(H1N1)pdm09 via aerosols (19). The 50% human infectious dose ($HID_{50}$) of aerosolized A(H1N1)pdm09 was taken to be 1-3 virions (26). To determine the expected time required for a A(H1N1)pdm09 case to shed 1 virion via aerosols, we took the reciprocal of the Poisson means and their 95% CIs at the different cps of the estimated shedding rates. The expected time required for a COVID-19 case to shed 1 virion via aerosols or 1 virion via droplets or aerosols was determined in a same manner.

**Data availability.** Data will be made available upon request. All raw data, code and model outputs from this study will be made publicly available in online repositories after peer review. Search strategies for the systematic review are shown in Supplementary Tables 1-5. The systematic review protocol was prospectively registered on PROSPERO (registration number, CRD42020204637).

**Acknowledgments**

We thank T. Alba (Toronto) for discussion on statistical methods. We thank J. Jimenez (Colorado) for discussion on the characteristics of aerosols and droplets. We thank E. Lavezzo and A. Chrisanti (Padova) and A. Wyllie, A. Ko and N. Grubaugh (Yale) for responses to data inquiries. This work was supported by the Natural Sciences and Engineering Research Council of Canada (NSERC) and the Toronto COVID-19 Action Fund. P.Z.C. was supported by the NSERC Vanier Scholarship (608544). D.N.F. was supported by the Canadian Institutes of Health

Research (Canadian COVID-19 Rapid Research Fund, OV4-170360). F.X.G. was supported by the NSERC Senior Industrial Research Chair.

**Author Contributions:** P.Z.C. designed research, analyzed data and wrote the paper. P.Z.C. and N.B. conducted screening, appraised studies and drafted the review protocol. Z.P. developed and conducted the systematic review search. M.K. and D.N.F. assessed methods, interpreted results and contributed to the discussion. All authors reviewed and revised the manuscript. F.X.G. supervised the research.

**Competing Interest Statement:** The authors declare no competing interest.

## References

1. E. Dong, H. Du, L. Gardner, An interactive web-based dashboard to track COVID-19 in real time. *Lancet Infect. Dis.* **20**, 533-534 (2020).
2. K. A. Prather *et al.*, Airborne transmission of SARS-CoV-2. *Science* **370**, 303-304 (2020).
3. C. J. Roy, D. K. Milton, Airborne transmission of communicable infection — the elusive pathway. *N. Engl. J. Med.* **350**, 1710-1712 (2004).
4. L. Liu, Y. Li, P. V. Nielsen, J. Wei, R. L. Jensen, Short-range airborne transmission of expiratory droplets between two people. *Indoor Air* **27**, 452-462 (2017).
5. J. J. Wei, Y. G. Li, Enhanced spread of expiratory droplets by turbulence in a cough jet. *Build. Environ.* **93**, 86-96 (2015).
6. D. K. Chu *et al.*, Physical distancing, face masks, and eye protection to prevent person-to-person transmission of SARS-CoV-2 and COVID-19: a systematic review and meta-analysis. *Lancet* **395**, 1973-1987 (2020).
7. S. Y. Park *et al.*, Coronavirus disease outbreak in call center, South Korea. *Emerg. Infect. Dis.* **26**, 1666-1670 (2020).
8. J. Y. Lu *et al.*, COVID-19 outbreak associated with air conditioning in restaurant, Guangzhou, China, 2020. *Emerg. Infect. Dis.* **26**, 1628-1631 (2020).
9. L. Hamner *et al.*, High SARS-CoV-2 attack rate following exposure at a choir practice - Skagit County, Washington, March 2020. *MMWR Morb. Mortal. Wkly. Rep.* **69**, 606-610 (2020).
10. Q. Li *et al.*, Early transmission dynamics in Wuhan, China, of novel coronavirus-infected pneumonia. *N. Engl. J. Med.* **382**, 1199-1207 (2020).

559 11. X. Hao *et al.*, Reconstruction of the full transmission dynamics of COVID-19 in Wuhan.
560 *Nature* **584**, 420-424 (2020).
561 12. R. Laxminarayan *et al.*, Epidemiology and transmission dynamics of COVID-19 in two
562 Indian states. *Science* **370**, 691-697 (2020).
563 13. A. Endo, S. Abbott, A. J. Kucharski, S. Funk, Estimating the overdispersion in COVID-
564 19 transmission using outbreak sizes outside China. *Wellcome Open Research* **5** (2020).
565 14. Q. Bi *et al.*, Epidemiology and transmission of COVID-19 in 391 cases and 1286 of their
566 close contacts in Shenzhen, China: a retrospective cohort study. *The Lancet Infectious*
567 *Diseases* **20**, 911-919 (2020).
568 15. J. O. Lloyd-Smith, S. J. Schreiber, P. E. Kopp, W. M. Getz, Superspreading and the effect
569 of individual variation on disease emergence. *Nature* **438**, 355-359 (2005).
570 16. M. G. Roberts, H. Nishiura, Early estimation of the reproduction number in the presence
571 of imported cases: pandemic influenza H1N1-2009 in New Zealand. *PLoS One* **6**, e17835
572 (2011).
573 17. J. Brugger, C. L. Althaus, Transmission of and susceptibility to seasonal influenza in
574 Switzerland from 2003 to 2015. *Epidemics* **30**, 100373 (2020).
575 18. I. T. Yu *et al.*, Evidence of airborne transmission of the severe acute respiratory
576 syndrome virus. *N. Engl. J. Med.* **350**, 1731-1739 (2004).
577 19. B. J. Cowling *et al.*, Aerosol transmission is an important mode of influenza A virus
578 spread. *Nature Communications* **4**, 1935 (2013).
579 20. E. C. Lee, N. I. Wada, M. K. Grabowski, E. S. Gurley, J. Lessler, The engines of SARS-
580 CoV-2 spread. *Science* **370**, 406-407 (2020).

21. R. Wolfel *et al.*, Virological assessment of hospitalized patients with COVID-2019. *Nature* **581**, 465-469 (2020).

22. M. M. Arons *et al.*, Presymptomatic SARS-CoV-2 infections and transmission in a skilled nursing facility. *N. Engl. J. Med.* **382**, 2081-2090 (2020).

23. X. He *et al.*, Temporal dynamics in viral shedding and transmissibility of COVID-19. *Nat. Med.* **26**, 672-675 (2020).

24. V. E. Pitzer, G. M. Leung, M. Lipsitch, Estimating variability in the transmission of severe acute respiratory syndrome to household contacts in Hong Kong, China. *Am. J. Epidemiol.* **166**, 355-363 (2007).

25. D. K. Ip *et al.*, Viral shedding and transmission potential of asymptomatic and paucisymptomatic influenza virus infections in the community. *Clin. Infect. Dis.* **64**, 736-742 (2017).

26. P. Fabian *et al.*, Influenza virus in human exhaled breath: an observational study. *PLoS One* **3**, e2691 (2008).

27. J. Ma *et al.*, COVID-19 patients in earlier stages exhaled millions of SARS-CoV-2 per hour. *Clin. Infect. Dis.* 10.1093/cid/ciaa1283 (2020).

28. H. Y. Cheng *et al.*, Contact tracing assessment of COVID-19 transmission dynamics in Taiwan and risk at different exposure periods before and after symptom onset. *JAMA Intern Med* **180**, 1156-1163 (2020).

29. W. E. Wei *et al.*, Presymptomatic transmission of SARS-CoV-2 — Singapore, January 23-March 16, 2020. *MMWR Morb. Mortal. Wkly. Rep.* **69**, 411-415 (2020).

30. Z. Du *et al.*, Serial interval of COVID-19 among publicly reported confirmed cases. *Emerg. Infect. Dis.* **26**, 1341-1343 (2020).

31. W. J. Guan *et al.*, Clinical characteristics of coronavirus disease 2019 in China. *N. Engl. J. Med.* **382**, 1708-1720 (2020).
32. R. Li *et al.*, Substantial undocumented infection facilitates the rapid dissemination of novel coronavirus (SARS-CoV-2). *Science* **368**, 489-493 (2020).
33. L. Luo *et al.*, Contact settings and risk for transmission in 3410 close contacts of patients with COVID-19 in Guangzhou, China: a prospective cohort study. *Ann. Intern. Med.* 10.7326/M20-2671 (2020).
34. X. Lu *et al.*, SARS-CoV-2 infection in children. *N. Engl. J. Med.* **382**, 1663-1665 (2020).
35. C. C.-R. Team, Coronavirus disease 2019 in children - United States, February 12-April 2, 2020. *MMWR Morb. Mortal. Wkly. Rep.* **69**, 422-426 (2020).
36. M. S. Han, J. H. Byun, Y. Cho, J. H. Rim, RT-PCR for SARS-CoV-2: quantitative versus qualitative. *Lancet Infect. Dis.* 10.1016/S1473-3099(20)30424-2 (2020).
37. H.-L. Yen *et al.*, Effect of voicing and articulation manner on aerosol particle emission during human speech. *PLoS One* **15** (2020).
38. J. J. A. van Kampen *et al.*, Shedding of infectious virus in hospitalized patients with coronavirus disease-2019 (COVID-19): duration and key determinants. medRxiv:10.1101/2020.06.08.20125310 (2020).
39. D. Moher, A. Liberati, J. Tetzlaff, D. G. Altman, P. Group, Preferred reporting items for systematic reviews and meta-analyses: the PRISMA statement. *PLoS Med.* **6**, e1000097 (2009).
40. J. P. T. Higgins *et al.* Cochrane handbook for systematic reviews of interventions. in *Cochrane book series* (John Wiley & Sons, 2019).

41. P. Warnke, L. Warning, A. Podbielski, Some are more equal - a comparative study on swab uptake and release of bacterial suspensions. *PLoS One* **9**, e102215 (2014).

42. E. Lavezzo *et al.*, Suppression of a SARS-CoV-2 outbreak in the Italian municipality of Vo'. *Nature* **584**, 425-429 (2020).

43. K. K. To *et al.*, Temporal profiles of viral load in posterior oropharyngeal saliva samples and serum antibody responses during infection by SARS-CoV-2: an observational cohort study. *Lancet Infect. Dis.* **20**, 565-574 (2020).

44. L. L. Poon *et al.*, Detection of SARS coronavirus in patients with severe acute respiratory syndrome by conventional and real-time quantitative reverse transcription-PCR assays. *Clin. Chem.* **50**, 67-72 (2004).

45. D. C. Adam *et al.*, Clustering and superspreading potential of SARS-CoV-2 infections in Hong Kong. *Nat. Med.* 10.1038/s41591-020-1092-0 (2020).

46. J. Riou, C. L. Althaus, Pattern of early human-to-human transmission of Wuhan 2019 novel coronavirus (2019-nCoV), December 2019 to January 2020. *Euro Surveill.* **25** (2020).

47. Y. Zhang, Y. Li, L. Wang, M. Li, X. Zhou, Evaluating transmission heterogeneity and super-spreading event of COVID-19 in a metropolis of China. *Int. J. Environ. Res. Public Health* **17**, 3705 (2020).

48. A. Tariq *et al.*, Real-time monitoring the transmission potential of COVID-19 in Singapore, March 2020. *BMC Med.* **18**, 166 (2020).

49. X. Wan, W. Wang, J. Liu, T. Tong, Estimating the sample mean and standard deviation from the sample size, median, range and/or interquartile range. *BMC Med. Res. Methodol.* **14**, 135 (2014).

649 50. P. Baccam, C. Beauchemin, C. A. Macken, F. G. Hayden, A. S. Perelson, Kinetics of
650 influenza A virus infection in humans. *J. Virol.* **80**, 7590-7599 (2006).
651 51. J. Yan *et al.*, Infectious virus in exhaled breath of symptomatic seasonal influenza cases
652 from a college community. *Proc. Natl. Acad. Sci. U. S. A.* **115**, 1081-1086 (2018).
653 52. L. L. Lau *et al.*, Viral shedding and clinical illness in naturally acquired influenza virus
654 infections. *J. Infect. Dis.* **201**, 1509-1516 (2010).
655 53. A. G. L'Huillier, G. Torriani, F. Pigny, L. Kaiser, I. Eckerle, Culture-competent SARS-
656 CoV-2 in nasopharynx of symptomatic neonates, children, and adolescents. *Emerg.*
657 *Infect. Dis.* **26**, 2494-2497 (2020).
658 54. H. W. Jeong *et al.*, Viable SARS-CoV-2 in various specimens from COVID-19 patients.
659 *Clin. Microbiol. Infect.* 10.1016/j.cmi.2020.07.020 (2020).
660 55. G. R. Johnson *et al.*, Modality of human expired aerosol size distributions. *J. Aerosol Sci*
661 **42**, 839-851 (2011).
662 56. L. Morawska *et al.*, Size distribution and sites of origin of droplets expelled from the
663 human respiratory tract during expiratory activities. *J. Aerosol Sci* **40**, 256-269 (2009).
664 57. S. Asadi *et al.*, Aerosol emission and superemission during human speech increase with
665 voice loudness. *Sci. Rep.* **9**, 2348 (2019).

666 **Figures**

667

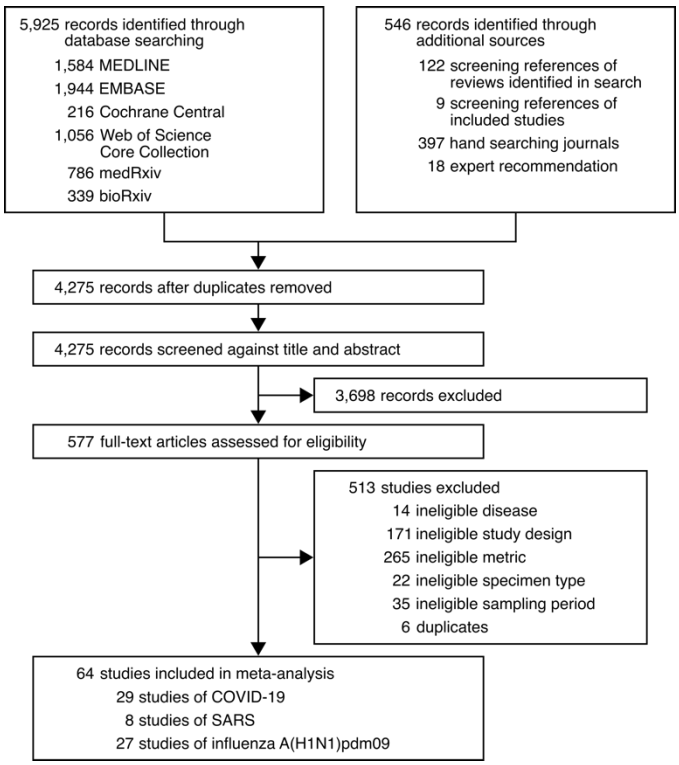


668

669

670 **Fig. 1.** Development of the systematic dataset.

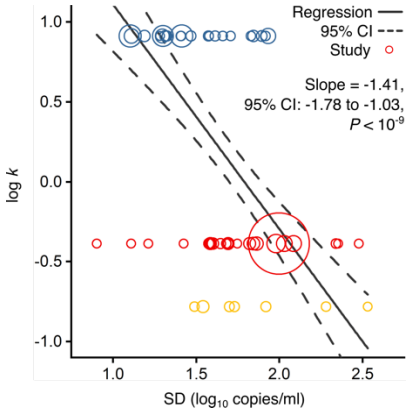


671

672

673 **Fig. 2.** Association of overdispersion in SARS-CoV-2, SARS-CoV-1 and A(H1N1)pdm09
674 transmissibility with heterogeneity in rVL. Meta-regression of dispersion parameter (*k*) with the
675 standard deviation (SD) of respiratory viral loads (rVLs) from contributing studies with low risk
676 of bias (Pearson's $r = -0.73$). Pooled estimates of k were determined from the literature for each
677 infection. Blue, red and yellow circles denote A(H1N1)pdm09 ($N = 22$), COVID-19 ($N = 24$)
678 and SARS ($N = 7$) studies, respectively. Circle sizes denote weighting in the meta-regression.
679 The *P*-value was obtained using the meta-regression slope *t*-test.

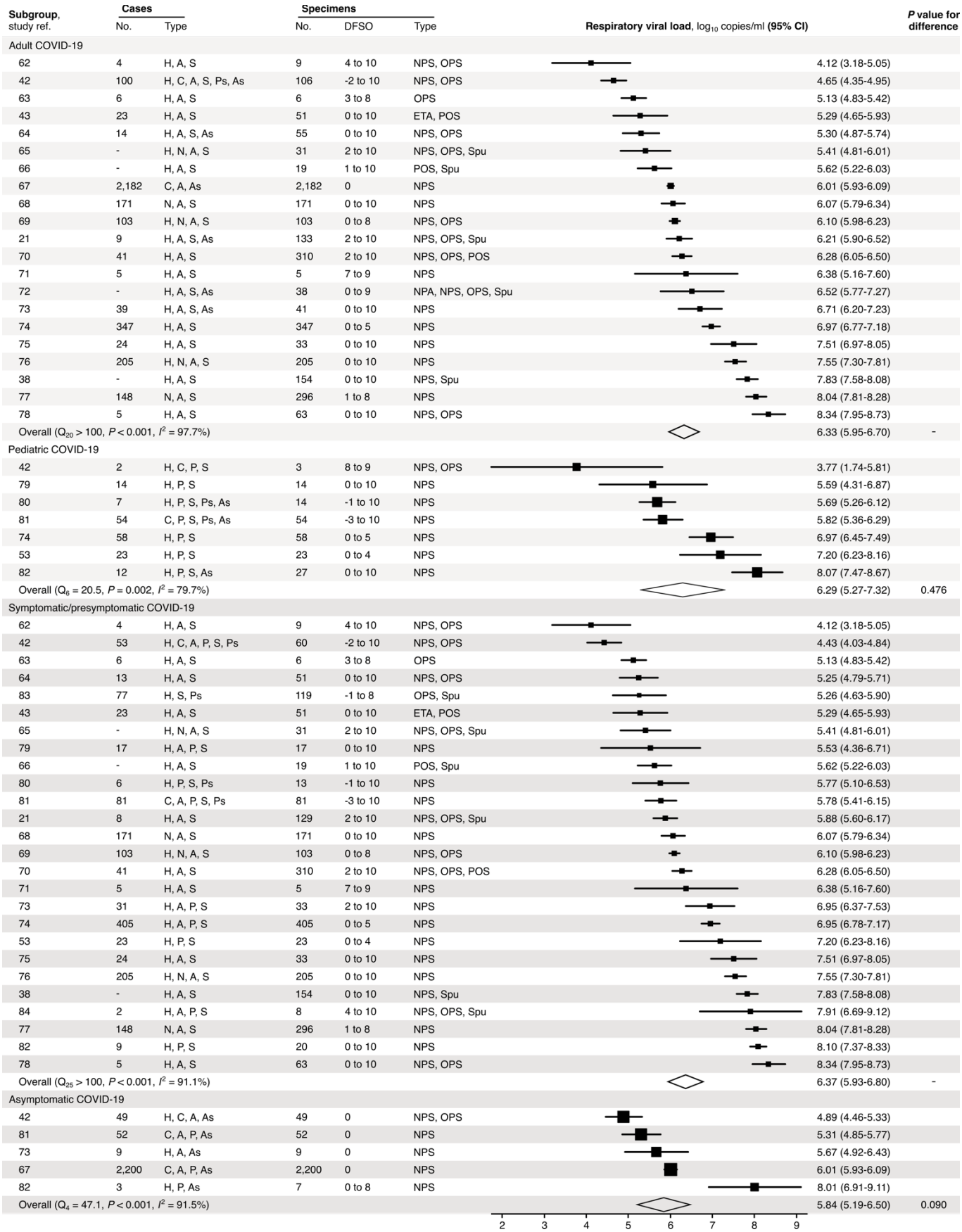


680

681

682 **Fig. 3.** Subgroup analyses of SARS-CoV-2 rVL during the infectious period. Random-effects
683 meta-analyses comparing the expected respiratory viral loads (rVLs) of adult (≥18 years old)
684 COVID-19 cases with pediatric (<18 years old) ones (top) and symptomatic/presymptomatic
685 infections with asymptomatic ones (bottom) during the infectious period. Quantitative rVLs refer
686 to virus concentrations in the respiratory tract. Case types: hospitalized (H), not admitted (N),
687 community (C), adult (A), pediatric (P), symptomatic (S), presymptomatic (Ps) and
688 asymptomatic (As). Specimen types: endotracheal aspirate (ETA), nasopharyngeal aspirate
689 (NPA), nasopharyngeal swab (NPS), oropharyngeal swab (OPS), posterior oropharyngeal saliva
690 (POS) and sputum (Spu). Dashes denote case numbers that were not obtained. Box sizes denote
691 weighting in the overall estimates. Between-study heterogeneity was assessed using the *P*-value
692 from Cochran's *Q* test and the $I^2$ statistic. References after 57 are listed in *SI Appendix*,
693 References. One-sided Welch's *t*-tests compared expected rVLs between the COVID-19
694 subgroups (non-significance, $P > 0.05$).

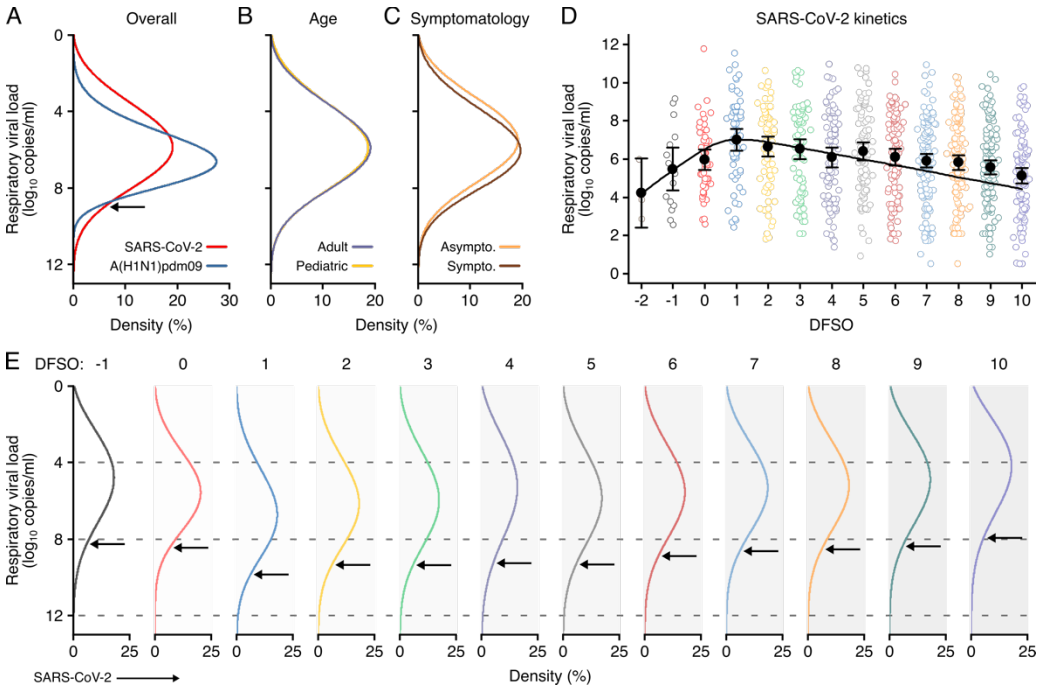


**Fig. 4. Heterogeneity and kinetics of SARS-CoV-2 rVL.** (*A*) Estimated distribution of respiratory viral load (rVL) for SARS-CoV-2 ($N = 3,834$ samples from $N = 26$ studies) and A(H1N1)pdm09 ($N = 512$ samples from $N = 10$ studies) throughout the infectious periods. (*B* and *C*) Estimated distribution of SARS-CoV-2 rVL for adult ($N = 3,575$ samples from $N = 20$ studies) and pediatric ($N = 198$ samples from $N = 9$ studies) (*B*) and symptomatic/presymptomatic ($N = 1,574$ samples from $N = 22$ studies) and asymptomatic ($N = 2,221$ samples from $N = 7$ studies) (*C*) COVID-19 cases. (*D*) SARS-CoV-2 rVLs fitted to a mechanistic model of viral kinetics (black curve, $r^2 = 0.84$ for mean estimates). Filled circles and bars depict mean estimates and 95% CIs. Open circles show the entirety of individual sample data over days from symptom onset (DFSO) (left to right, $N = 3$, 15, 50, 63, 71, 75, 85, 93, 105, 136, 123, 128 and 115 samples from $N = 21$ studies). (*E*) Estimated distributions of SARS-CoV-2 rVL across DFSO. Weibull distributions were fitted on the entirety of individual sample data

709 for the virus, subgroup or DFSO in the systematic dataset. Arrows denote 90$^{th}$ case percentiles

710 for SARS-CoV-2 rVL distributions.

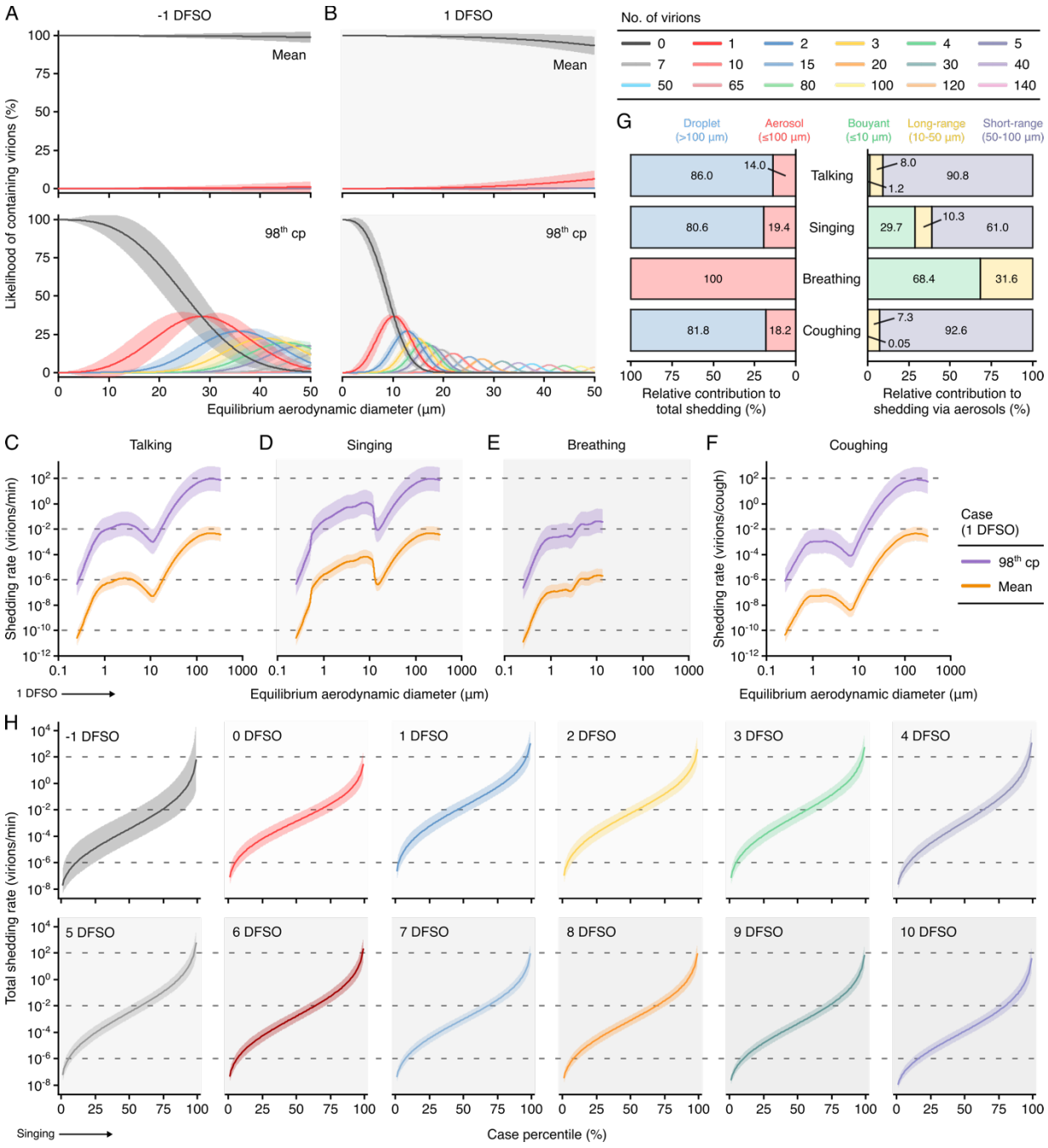


**Fig. 5.** Heterogeneity in shedding SARS-CoV-2 via droplets and aerosols. (*A* and *B*) Estimated likelihood of respiratory particles containing viable SARS-CoV-2 when expelled by the mean (top) or 98$^{th}$ case percentile (cp) (bottom) COVID-19 cases at -1 (*A*) or 1 (*B*) days from symptom onset (DFSO). For higher no. of virions, some likelihood curves were omitted to aid

visualization. When the likelihood for 0 virions approaches 0%, particles are expected to contain at least one viable copy. (*C* to *F*) Rate that the mean and 98$^{th}$-cp COVID-19 cases at 1 DFSO shed viable SARS-CoV-2 by talking, singing, breathing or coughing over particle size. (*G*) Relative contributions of droplets and aerosols to shedding virions for each respiratory activity (left). Relative contribution of buoyant, long-range and short-range aerosols to shedding virions via aerosols for each respiratory activity (right). (*H*) Case heterogeneity in the total shedding rate (over all particle sizes) of virions via singing across the infectious period. Earlier presymptomatic days were excluded based on limited data. Data range between the 1$^{st}$ and 99$^{th}$ cps. Lines and bands represent estimates and 95% CIs, respectively, for estimated likelihoods or Poisson means.